Surface water connectivity dynamics of a large scale extreme flood

Mark A Trigg [a,*]

Katerina Michaelides [a]

Jeffrey C Neal [a]

Paul D Bates [a]

[*] Corresponding author: Tel: +44 (0)117 928 8290; Fax: +44 (0)117 928 7878; E-mail address: mark.trigg@bristol.ac.uk

[a] Hydrology Group, School of Geographical Sciences, University of Bristol, University Road, Bristol, BS8 1SS, UK.

Abstract

During flood inundation, river water passes from the main channel into the floodplain through floodplain channels and diffusive overbank flow. This flood water is then distributed within the floodplain depending upon internal connections, barriers and storage, and finally returns back to the river through drainage connections. This surface water connectivity can be complex and is important to many aspects of floodplain functioning, including ecology, sediment movement and flood risk. However, there is currently no accepted way of quantifying this connectivity objectively. We quantify surface water connectivity geostatistically as an objectively measurable characteristic of an observed flood event using a time series of MODIS (Moderate Resolution Imaging Spectroradiometer) surface water product for an extreme large scale flood event (11,000 km^2 flooded area and 6 month duration) during 2011 in Bangkok, Thailand. We develop and apply a new gap filling method that better preserves the dynamic information of the event than simple aggregation methods. Comparison of MODIS results with the higher resolution Earth Observer 1 shows fundamental differences in the resolved connectivity with scale despite similar flooded area. The effect of the passage of the flood wave is directly observable in the river reach, as out-of-bank flooding progresses and increases connectivity along the river during rising water. Around peak flow, there is an increase in connectivity of the floodplain adjacent to the river as low lying areas fill. A step increase in connectivity is correlated with a major levee breach. During recession there is a rapid reduction in along river connectivity in the first week after the peak. This rapid reduction contrasted with a slow decrease in the floodplain connectivity as flooded depressions gradually drained reducing depth, while flood extent remained static for long periods. The connectivity analysis of the threshold in floodplain draining indicates that although spatial flood extent changes are small at this time, there is a reorganisation of the internal surface water connectivity within the flooded area. Thus through this measure of connectivity, we can see a clear structure to the event progression with new insights into flood dynamics that were not anticipated *a priori*.

Keywords

Geostatistical Connectivity; Floodplain dynamics; 2011 Bangkok, Thailand; MODIS

1 Introduction

Connectivity in this paper refers to the dynamic flow interactions between a river and its floodplain, as well as between different areas within the floodplain. During large floods these flow connections occur through two main surface water processes, channelized flow through floodplain channels and diffusive overbank flow. To a lesser extent, but still important in some systems are groundwater flow connections and evaporation. The timings and flow input through floodplain channels and diffusive overbank flow affect the rate of floodplain filling and the final extent of inundation. The relative difference between water levels and channel bed and bank elevations controls flow rates and provides connection and disconnection thresholds within the system. Thus the movement of flood water from the river to the floodplain, within the floodplain, and back to the river is strongly dependent on how connected the two bodies are. This surface water connectivity can be complex and arises from the physical topography of the system (e.g. channels and topographic barriers) as well as dynamic hydraulic gradients from the passage of the flood wave. For a detailed description and discussion of the floodplain inundation and recession sequence, we refer the reader to Zwolinski (1992).

Surface water connectivity during inundation has been identified as important to many aspects of a floodplain's functioning. For example, the flood pulse concept introduced by Junk et al. (1989) and extended by Tockner et al. (2000) shows that floodplain habitat heterogeneity is mainly a product of shifting water sources and different flow paths as well as the relative importance of autogenic processes. Disruption to the connectivity that is vital to ecology and river management schemes invariably leads to reductions in biodiversity (Ward and Stanford, 1995; Ward et al., 1999; Pringle, 2001). Floodplain channels providing important sediment distribution pathways onto a floodplain (Mertes et al., 1996; Day et al., 2008) as well as the deposition and erosion of sediment altering the structure and morphology of floodplain (Trigg et al., 2012), thus connectivity is both created by, and creates, the morphology of the floodplain. Flow connectivity between the river and its floodplain, as well as within the floodplain, has important consequences for flood risk management and river engineering (Gilvear, 1999). Floodplains that are well connected to the river channels provide water storage progressively during the rising limb of an event which reduces peak flood flows and levels, and, conversely, an artificially confined river with poor connectivity leads to higher channel water levels and the danger of sudden and catastrophic flooding through levee collapse or overtopping.

Despite the accepted importance of floodplain flow connectivity for flood dynamics, it has thus far been challenging to quantify due to a lack of event data of sufficiently detailed spatial and temporal resolution. However, recent advances in remote sensing datasets and new processing methods are providing new opportunities to study rivers and their floodplains at unprecedented levels of spatial and temporal detail (Smith, 1997; Marcus and Fonstad, 2010). Also, increasingly, remotely sensed flood extent data are being successfully used to build, calibrate and validate complex large scale hydraulic models where the correct representation of dynamic flow processes are crucial (e.g. Bates et al., 2006; Wilson et al., 2007; Schumann et al., 2011; Bates, 2012; Neal et al., 2012). In addition, these remote sensing data are now being made readily available pre-processed, allowing wider use within the hydrological community. One such flood extent dataset is that provided by Dartmouth Flood Observatory (DFO), derived from the internationally available and free rapid response data from NASA's two MODIS (Moderate-resolution Imaging Spectroradiometer) sensors (Brakenridge and Anderson, 2006). DFO in collaboration with NASA have been processing and archiving imagery acquired twice daily for several years and these data are made freely available at their websites. These datasets can also provide new opportunities to apply new analysis methods that were not previously possible due to lack of data at sufficient temporal and spatial resolutions.

The availability of sequences of flood extent provided by these methods are now allowing the validation of hydraulic models through a wider dynamic range of an event (Bates et al., 2006; Schumann et al., 2011), rather than just at a single point in the event, as well as being used in near

real time to monitor floods (Chien et al., 2011; Auynirundronkool et al., 2012; McLaren et al., 2012). There are many potentially important flow processes active on a floodplain, such as floodplain channels and ditches providing flow connections (Nicholas and Mitchell, 2003) as well as barriers such as embankments, floodplain channel levees and woody debris blocking flow connections (Jeffiries et al., 2003). If a model lacks sufficient detail in the topography data used to represent the floodplain, many of these connection details of the floodplain system can be missing (Trigg et al., 2012) and this commonly leads models having difficulties in filling and draining the floodplain at the correct point in the flood cycle (Wilson et al., 2007; Neal et al., 2011). The increasing availability of airborne laser altimetry (LiDAR) data has been shown to improve connectivity within flood models, although Bates et al. (2003) note that its optimum assimilation requires good flood observation data to discriminating between competing approaches. In addition, these connection/ disconnection processes can occur at different times during the event and at different threshold levels and locations, and may only be active in the rising or recession periods of an event. Thus this wealth of new temporal and spatial flood observation data can help with the assessment of what flow processes are important during a flood and at which scales, presenting opportunities for the modeller to understand and improve the process representation within models.

Within flood dynamics related research, there is a growing body of research that focuses on connectivity to biodiversity (Ward et al., 1999), lake levels (Pavelsky and Smith, 2008), hillslope runoff and geomorphology (Bracken and Croke, 2007; Smith et al., 2010). However, we are unaware of any research attempting to specifically quantify connectivity as an objectively measurable characteristic of an observed flood event. Indeed, the lack of universal measures of river-floodplain connectivity limits the comparison of the response of aquatic assemblages to hydrological connectivity and impedes the understanding of floodplain functioning across different systems (Gallardo et al., 2009). Although it is possible to assess connectivity of a particular part of a floodplain by measures such as time or duration of connection, water levels synchronous within adjacent areas etc. (e.g. Karim et al., 2012), all these measures suffer from a location and scale specific bias. Recent work has developed frameworks for more robust and objective quantification of connectivity based on spatial data that transcend individual complexities in hydrological response and that allow comparisons between locations and events (Pardo-Iguzquiza and Dowd, 2003); Michaelides and Chappell (2009).

In this paper we use geostatistical connectivity analysis in conjunction with remotely sensed flood data from MODIS (Moderate Resolution Imaging Spectroradiometer) and Earth Observer 1 (EO-1, Advanced Land Imager (ALI)) for the large scale (11,000 km^2 flooded area and 6 month duration) flood event that occurred during 2011 in Bangkok, Thailand. The geostatistical connectivity function quantifies the probability that any two points separated by a specified distance are connected and hence enables mapping of the points and their likelihood in being connected to a specific location (Pardo-Iguzquiza and Dowd, 2003). The aim of this paper is to quantify the observed spatial and temporal changes in surface water connectivity on the floodplain in order to provide insights into flood dynamics. We also assess geostatistical connectivity as a tool for quantification of flood dynamics and evaluate the utility of the MODIS flood mapping product for a post-event analysis of a time-series of flood extents, exploring issues such as data completeness and spatial and temporal event scales.

2 Methodology and Data

2.1 Geostatistical connectivity

The geostatistical connectivity function is a multi-point statistic based on binary state data which quantifies the probability that any two points separated by a specified distance are connected and hence enables mapping of points and the likelihood of their connection to a specific location (Pardo-Iguzquiza and Dowd, 2003). This function, therefore, quantifies the more subtle differences in the data fields associated with increasing connectedness and spatial organisation, and enables characterisation of spatio-temporal patterns that can be used to interpret transitions and thresholds in flow processes (Michaelides and Chappell, 2009).

The connectivity function expresses the probability that n points along a given direction are all valued above the threshold value z_c (Journel et al., 2000):

$$P(n; z_c) = \mathbf{Pr}\left\{\prod_{j=1}^{n} I(\mathbf{u}_j; z_c) = 1\right\} \quad \textbf{(1)}$$

where $I(\mathbf{u}_j;z_c)$ is an indicator of the variable $Z(\mathbf{u}_j)$ at location $\mathbf{u}_j$ that exceeds the threshold value z_c, defined as $I(\mathbf{u}_j;z_c) = 1$ if $Z(\mathbf{u}_j) > z_c$, zero if not, and $\prod$ is the product operator. It is estimated when the starting location $\mathbf{u}_1$ takes all possible positions within the field. The greater the spatial entropy of the field, the faster the decrease to zero of $P(n;z_c)$ as n increases. Thus the value of the connectivity function at any given distance is the fraction of points along a given direction at that distance that are connected.

The connectivity analysis applied in this paper is based on a Matlab rewrite of the FORTRAN software CONNEC3D developed by Pardo-Iguzquiza and Dowd (2003). The Matlab connectivity function is provided with this paper as supplementary material. The software performs the analysis on a 2D binary grid of cells and calculates the connectivity function for a chosen binary phase (e.g. 0 or 1) in four directions, along the two orthogonals (North-South and West-East) and the two diagonals (NW-SE and NE-SW). As well as the outputting the connectivity function itself, the analysis also results in metadata regarding the images analysed: the number of connected components (ncc), the average size of a connected component (cc), the mean length of a cc in the N-S and W-E directions, the size of the largest cc, the maximum length of a cc along N-S, W-E directions and the numbers of percolating components (components that connect from one edge of the analysis domain to the other) along N-S, W-E directions. In addition, the program provides as output a grid in which each cc is identified by an integer number ranging from 1 to ncc. Analysis can use 4-way connectivity (D4), which assumes cells connect by shared edge only or 8-way connectivity (D8), which allows cells to connect by edge and corner vertex.

The application of geostatistical connectivity in one direction to a very simple binary grid of 9 cells is illustrated in figure 1. This highlights some key aspects of the application of geostatistical connectivity to flood extent data sets:

(1) The analysis is based on the assumption that the binary grid of cells represents a wet/dry binary characterisation of flooding. This could be from a model output or observed data. Analysis is applied to the wet cells only, i.e. there is no explicit representation of flow depth.
(2) The analysis identifies all the separate (i.e. not connected) objects on the floodplain. This shows which flooded areas are connected and which are not, in terms of the binary map provided. Note, all wet cells that connect along any pathway (including non-direct routes) are considered part of the same connected object.
(3) Assuming at least one cell is wet; the connectivity function always starts at a value of 1 at zero distance because a wet cell is always connected to itself.

(4) The value of the connectivity function at any given distance is the fraction of wet cell pairs at that distance that are connected. Thus, a connectivity function value of 0.5 at 100 m would mean that half of the wet pairs of cells 100 m apart are connected. This also means the connectivity function value can never be greater than 1 (all wet cell pairs are connected).

(5) The distance at which the connectivity function finally reaches zero is the maximum length of any of the "strips" of connected cells in the analysis direction (even if there are gaps in the strips because the connection is via a parallel strip) (figure 1d).

(6) The connectivity function will eventually decrease with distance to zero. However, connectivity function can decrease and then increase again with distance. This means that a larger fraction of the wet cell pairs at the greater distance are connected, not that there are more wet cells at that distance. (figure 1b).

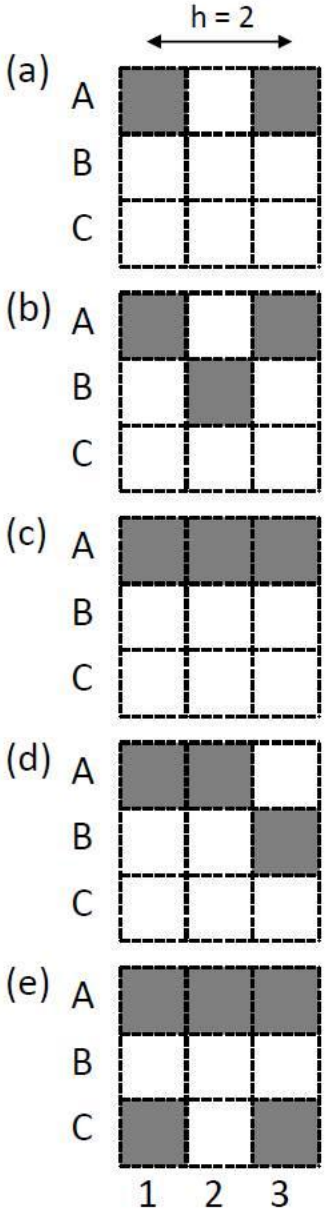

$CF_{(h=0)} = 1$
$CF_{(h=1)} = 0$
$CF_{(h=2)} = 0$

(a) No pairs of wet cells at h=1, so $CF_{(h=1)} = 0$. There is one pair (A1-A3) of wet cells at h=2, but they are not connected, so $CF_{(h=2)} = 0/1$.

$CF_{(h=0)} = 1$
$CF_{(h=1)} = 0$
$CF_{(h=2)} = 1$

(b) $CF_{(h=1)}$ remains zero as there are no pairs of wet cells in the x direction. However, A1-A3 are now connected by B2 and $CF_{(h=2)} = 1/1 = 1$.

$CF_{(h=0)} = 1$
$CF_{(h=1)} = 1$
$CF_{(h=2)} = 1$

(c) Now $CF_{(h=1)} = 2/2 = 1$ as there are two pairs (A1-A2 and A2-A3) of connected wet cells in the x direction at this distance. Also A1-A3 are now connected by A2 so $CF_{(h=2)} = 1/1 = 1$.

$CF_{(h=0)} = 1$
$CF_{(h=1)} = 1$
$CF_{(h=2)} = 0$

(d) Only one pair of cells at h=1 and they are connected so $CF_{(h=1)} = 1/1 = 1$. A1-B3 are connected (by A2) but there are no pairs at h=2 in the x direction so $CF_{(h=2)} = 0$.

$CF_{(h=0)} = 1$
$CF_{(h=1)} = 1$
$CF_{(h=2)} = 0.5$

(e) Like (c) there are two pairs at h=1, so ($CF_{(h=1)} = 2/2 = 1$. At distance h=2, there are two pairs of wet cells (A1-A3 and C1-C3), but only one of them is connected, so $CF_{(h=2)} = 1/2 = 0.5$.

Figure 1 - Illustration of the connectivity function (CF) in the X direction (West-East), assuming 8-way connectivity. Grey shaded cells are wet and white cells are dry. CF(h)= (pairs of connected wet cells / pairs of wet cells) at distance h apart for the direction under consideration.

For the application of geostatistical connectivity to the Bangkok flood, we used wet-dry binary raster grids derived from the remote sensing data observations, and assessed using 8-way connectivity. As the Bangkok flood was principally an event draining North to South, with floodplains on the West and East, we only present results in this paper for the surface water connectivity in the N-S and W-E directions.

2.2 Site and event description

We analysed an extreme flood event that took place in Thailand from July 2011 and lasting through to February 2012. The 2011 flood was the maximum ever recorded in Thailand (Komori et al., 2012), and predominantly involved the Chao Phraya River which drains 30% of the country and passes from the North of the country through a topographical narrowing at Nakhon Sawan and then through to the low-lying and relatively flat coastal plain that contains Bangkok city (Figure 2). This flood caused tremendous damage, including 813 dead nationwide, inundation damage and business interruption to seven industrial estates and 804 companies, and total losses estimated at 43 billion dollars (Komori et al., 2012).

The event began at the end of July 2011, with unusually heavy monsoon rains and a tropical cyclone bringing 143% of average monsoon seasonal rainfall (Komori et al., 2012), swelling rivers and filling reservoirs throughout the country. The flow in the Chao Phraya River entering the Bangkok coastal plain at Nakhon Sawan peaked at 4,686 m^3/s on 14 October 2011 with the floods reaching Bangkok city mainly through the Chao Phraya River as well as numerous canals and smaller waterways by 25 October 2011. The downstream part of the Chao Phraya River has diminished flow capacity, causing floodwater to pool in low lying areas adjacent to the river and tributaries to flood due to backwater effects preventing their drainage. A series of high tides at the end of October prevented the draining of the floodwaters to the sea and exacerbated flooding further, resulting in maximum flood extent around the 3 November 2011. Flood waters and full-to-capacity dams then slowly drained until January 2012. (Komori et al. (2012) provide a detailed hydrological review of the event).

The study area for this analysis (Figure 2) was confined to the lower plains of the Chao Phraya River, below Nakhon Sawan, defined by the 30 m elevation contour (~30,000 km^2). A set back from the coast of 25 km was used to exclude the low lying areas on the very edge of the coast as they are not part of the river flooding that is being assessed. Flow data for comparison with the flood extent in the lower plains (Figure 3) were downloaded for the Nakhon Sawan gauging station from the Thailand Royal Irrigation Department website (http://water.rid.go.th/). The bankfull discharge capacity of the lower watershed of the Chao Phraya River (to sea) above which flooding occurs in the lower plains is ~2,000 m^3/s (Komori et al., 2012).

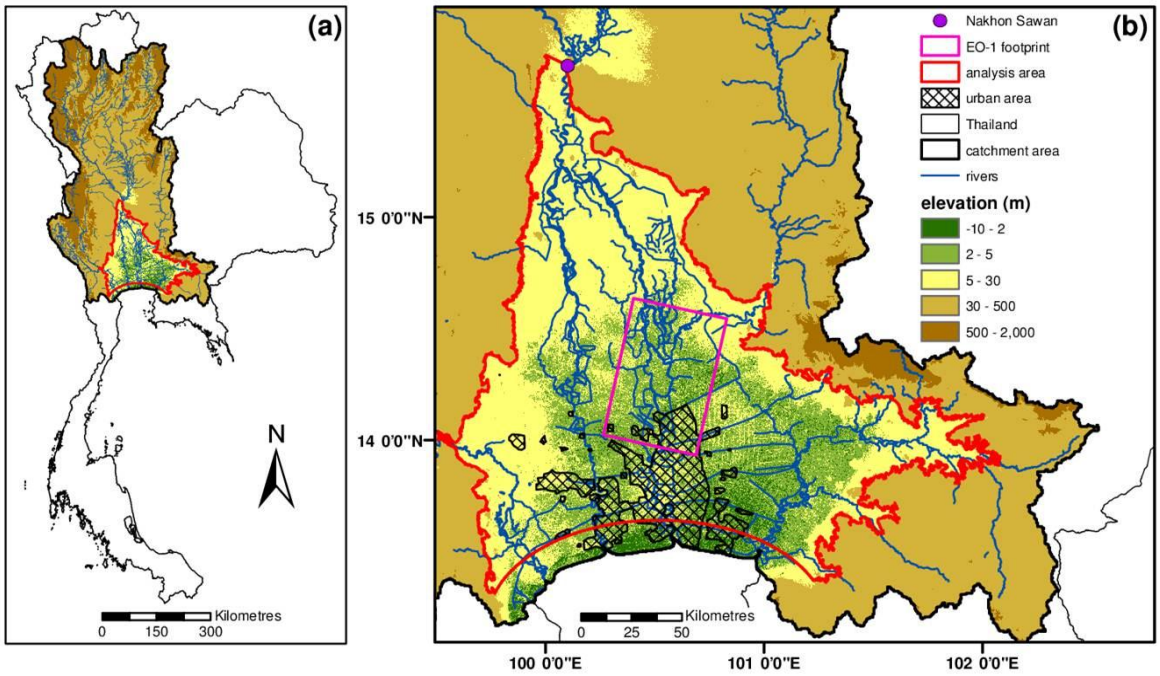

Figure 2 – Study area (a) Location of basin within Thailand. (b) Detailed inset of the analysis area defined by 30 m elevation contour and offset of 25 km from coast. Also shows Nakhon Sawan gauging station, the Bangkok City central urban area, main rivers, elevation and image EO-1 footprint.

2.3 MODIS data

Connectivity analysis of the extreme flood event over 203 days was carried out using MODIS data. The MODIS (Moderate Resolution Imaging Spectroradiometer) near real-time global flood mapping project, operated by NASA Goddard's Office of Applied Science, produces global daily surface and flood water maps at approximately 250 m resolution, in 10x10 degree tiles (http://oas.gsfc.nasa.gov/floodmap/home.html). The flood water maps build on the efforts of the Dartmouth Flood Observatory (DFO) to map floodwater extent in detail for floods in near real-time (http://floodobservatory.colorado.edu/). The data used for this study were downloaded from the DFO website (Brakenridge et al., 2012).

Flood mapping with the MODIS data is based on twice daily, wide-swath space-borne optical sensors, operating at a spatial resolution of 250 m (Syvitski et al., 2012). An automated processing algorithm for the MODIS band 1 and 2 data from instruments aboard NASA's Terra and Aqua spacecraft provides near-real time measurements of floodplain inundation (Brakenridge and Anderson, 2006). The algorithm used to produce the data for 2011, uses four images (Terra and Aqua, each day, for two days). A cloud shadow filter removes this source of error (shadow can otherwise be misclassified as water), and a filling process takes advantage of moving cloud obscuration to increase spatial coverage. Use of the two day composite thus sacrifices some temporal resolution but provides more complete spatial coverage and less "false positive" water classification error. During flood events, the evolving flood wave can be tracked down the basin through a moving flood extent, or the data can be aggregated temporally to provide total inundation over the event.

For the 2011 Bangkok flood event, there are two data products available from the NASA Goddard MODIS Global Flood Mapping Project: (1) MFW: MODIS Flood Water and (2) MSW: MODIS Surface Water (MFW before subtracting the reference water which is usually inundated, e.g. lakes.). We used the MSW product as we were interested in the connectivity of the rivers and floodwaters. The data files are identified using a year and day of year stamp, YYYYDOY. Where YYYY is a 4-digit year and DOY is a 3-digit day of year (001 to 365 or 366). The products are multi-day aggregates, to reduce issues of cloud cover. The product date is the last day of the composite period, so for the standard two day composite we used (2D2OT: 2 Days imagery, 2 Observations required, Terrain shadow masking applied), a product dated 2012015 includes data from the day before i.e. 2012014, and 2012015. The product is available as a vector dataset, with polygons covering identified wet areas.

The MODIS global flood mapping data used extended from 14 August 2011 (2011226) to 3 March 2012 (2012063). This covered the period from before out-of-bank flooding began, to well after drainage of the lower plains below Nakhon Sawan. The study area covers two 10 degree product tiles (mostly 100E020N with some to the West on 090E020N), which were merged, reprojected to a local UTM 47N co-ordinate system and converted to binary rasters (1 denoting wet and 0 dry/unknown) before analysis. There are 203 days in the analysis period, but only 176 of these had any MODIS flood data available, with missing data presumably due to complete cloud cover for the two day composite period. Even days with data available are not necessarily complete spatial coverages and can contain gaps due to clouds. Data completeness is important when analysing the dynamics of a flood event, so some way of assessing what is missing and, if possible, accounting for it is needed. As no information regarding missing data due to clouds or shadows is provided with the MODIS floodmap data for the Bangkok 2011 flood event, a visual assessment of the raw MODIS images was undertaken to qualitatively assess the cloud cover for the assessment area for the dataset. From this assessment, a low cloud dataset was identified. It should be noted here that a missing data flag is now provided in the new raster product (MWP – MODIS Water Product) as of March 2012. A common method employed to allow for missing data when using MODIS data is to aggregate the data for a period longer than two days, such as 8 or 16 days (e.g. Xiao et al., 2005). We created one and two week aggregate datasets using this method for analysis.

As well as analysing low cloud/high quality data days and weekly and two weekly aggregates, we developed and applied an alternative “gap-filling” method to account for missing data that utilises knowledge of typical flood dynamics. The method fills gaps in the time series of data by allowing for the fact that a given area is unlikely to be wet one day, dry the next and then wet again the following day. Thus the non-wet day/s (dry or missing data) in-between two wet days is marked as likely to be wet and included as wet in the infilled dataset. This gap filling method uses the full time series dataset of the flood event and includes days with no data by assuming all cells in those images are missing data. Each cell is examined in turn, starting at the beginning of the time series. Once a cell is wet, the length of gap in days to the next time the cell is wet is counted. If the time gap is smaller than the chosen infill gap period, then all the missing days in the period are marked as probably wet so that it can be included in the flooded area analysis. A detailed analysis of where and when the gaps occur in the dataset (i.e. gap structure) was undertaken and a full time series of gap filled extents was produced for 6, 13 and 27 day gap intervals, i.e. 1, 2, 4 weeks.

2.4 EO-1 processing

In order to provide a high resolution comparison to the MODIS 250 m resolution product, an Earth Observer 1 (EO-1, Advanced Land Imager (ALI)) image at 30 m resolution was used. The image from 26 November 2011, covering part of the North of Bangkok city (image footprint in figure 2), shows near peak flood extent and is cloud free. The EO-1 image was obtained from USGS EarthExplorer website (http://earthexplorer.usgs.gov/). Initial standard Normalised Difference Water Index (NDWI) processing (McFeeters, 1996) revealed issues resolving the wet areas where there were significant

urban structures. Instead, application of the modified method (MNDWI) (Xu, 2006) to allow for the urban effect was applied to derive a wet/dry binary raster.

3 Results

3.1 Flooded area

A time series of flooded area over the Bangkok basin for the full event gives a good overview of the quality of the original MODIS product as well as allowing comparison with that of the various aggregation and gap filled datasets (Figure 3). As would be expected for a flood event on this scale, the peak flood extent lags the peak input flow to the system by ~3-4 weeks. The original flood area for the MODIS product dataset shows large and hydraulically inconsistent variation in flood area from day to day throughout the event. This is related to cloud obscuring the images and is a well explained and understood aspect of MODIS data. It should be noted here that recently the Flood Observatory product is also provided routinely as a 14 day, running forward composite to address this issue.

The low cloud dataset represents a subset of the MODIS product which coincides with the outside envelope of the flooded area (Figure 3) and is useful in identifying the most complete images. From August to early October, monsoon weather patterns and the resulting clouds obscure the image on many days during the rising limb of the event, resulting in many data gaps. From the end of October through November, clouds are less common and there are more clear periods. Finally, December to March has patchy cloud resulting in numerous gaps again.

Summing all wet pixels for the entire event results in a total event flooded area of 11,000 km^2. While useful for an overall scale of the flooding, this number does not capture the dynamic aspects of the event. The low cloud dataset shows a peak flooded area during the event of 7,670 km^2 on the 3 November 2011 (week 45, 2011). However, close inspection of low cloud days shows there are still some missing areas of data from one day to the next, which appear, disappear and reappear inconsistently in a manner unlikely to be linked to the dynamics of such a smoothly increasing and decreasing flood event over such a long timescale. The data aggregation methods attempt to overcome this missing data problem and result in a larger flooded area for all weeks in the event. Data aggregated to one week results in a peak flood extent of 9,260 km^2 and 9,810 km^2 for a 2 week aggregate. The weekly aggregate time series shows a drop in flooded area for week 40, 2011 that is inconsistent with the flow input and our expectation of a steadily increasing event, and this reflects the fact there are very few parts of the study area unaffected by clouds for that week.

Results from the gap filling method also show an increase in flooded area throughout the event, although not as pronounced as the aggregation method and with a smoother transition from one week to the next. The peak flooded areas are 8,320, 8,690 and 8,940 km^2 for the 6, 13 and 27 day gap size filled datasets respectively.

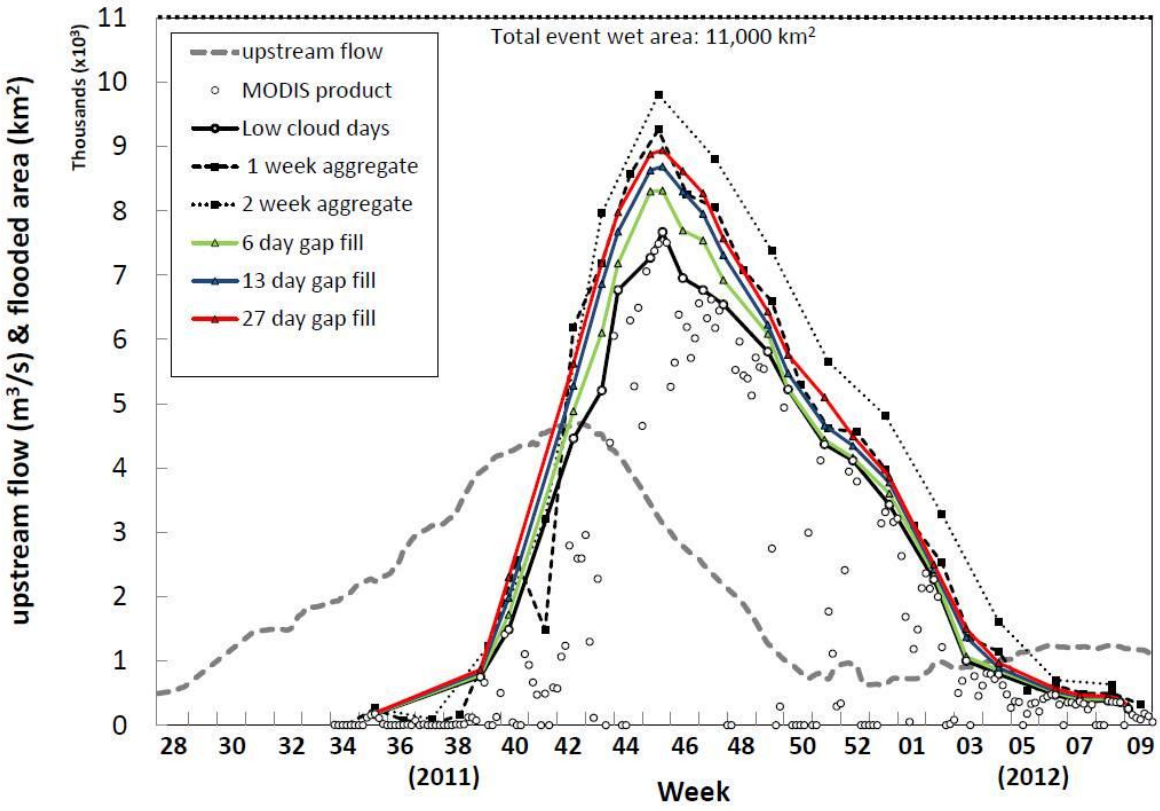

Figure 3 - Flooded areas for the analysis datasets and flow hydrograph. Upstream flow is the main inflow to the Bangkok basin measured at Nakhon Sawan gauging station. Note, only areas for low cloud days are shown for the low cloud and gap filled dataset plots.

Summing the wet pixels from daily flood extent data, using the 13 day gap filled dataset for illustration purposes, allows an examination of flood duration for the study area (Figure 4). The areas subject to the longest duration of flooding coincide with the low elevation bowl shaped depressions in the floodplain to the Northwest of the city, but also areas to the East of the main river channel in the North of the study area. Some of these areas provide flood storage on an almost annual basis; however the duration of this event and limited ability of the river to remove the flood water extended the area of the flooding severely.

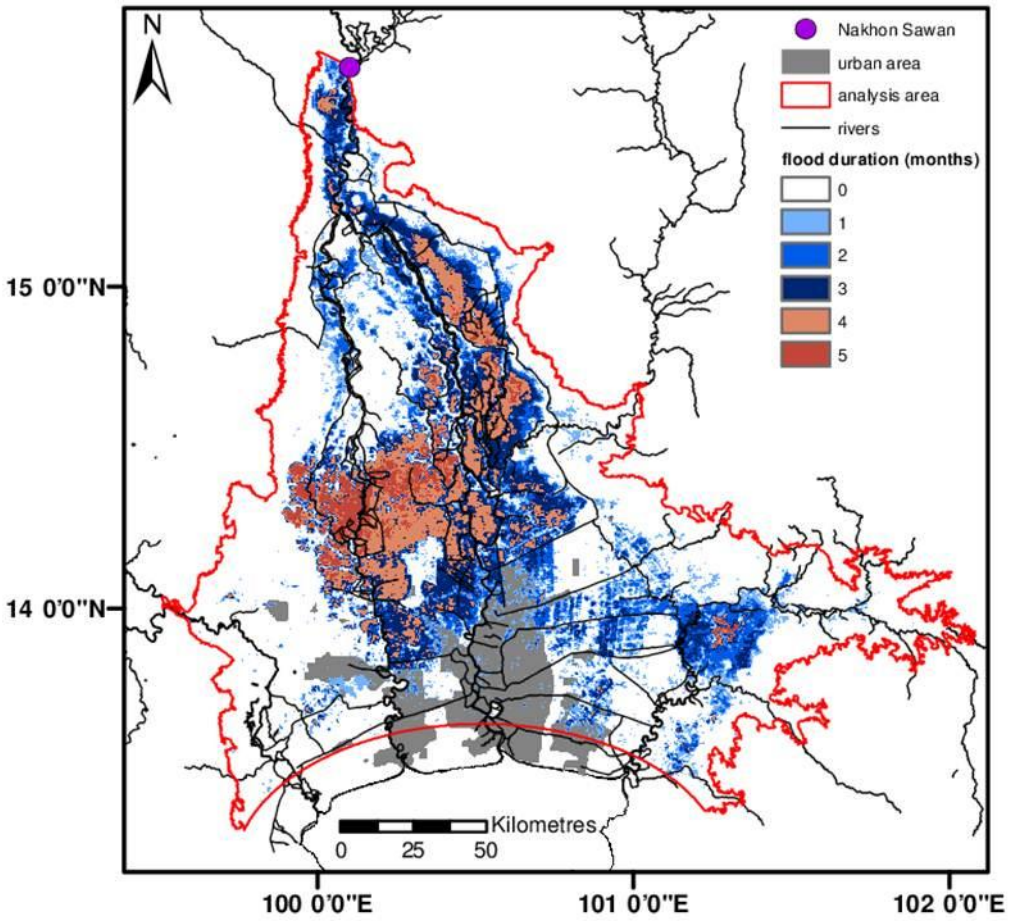

Figure 4 – Flooded duration in months derived from the 13 day gap fill dataset.

3.2 Surface water connectivity

Application of geostatistical connectivity analysis to the MODIS product data results in a series of connectivity function curves that reflect the continually changing connectivity of the surface water flooding throughout the event. For clarity, this is illustrated for three key points during the flood hydrograph in Figure 5, mid-rising, peak and mid-recession. As expected, the highest flow connectivity occurs during the flood peak. N-S flow connectivity extends over a longer distance (the point at which the connectivity function reaches zero on the axis) than W-E connectivity, due to the North-South orientation of the main river. Comparing the rising limb with the recession limb inundation extents shows the progression of the flood from the North of the area to the centre, in line with the movement of the flood wave southwards. The well connected large bodies of water show clearly the dominant inundated areas (black and red to yellow in Figure 5).

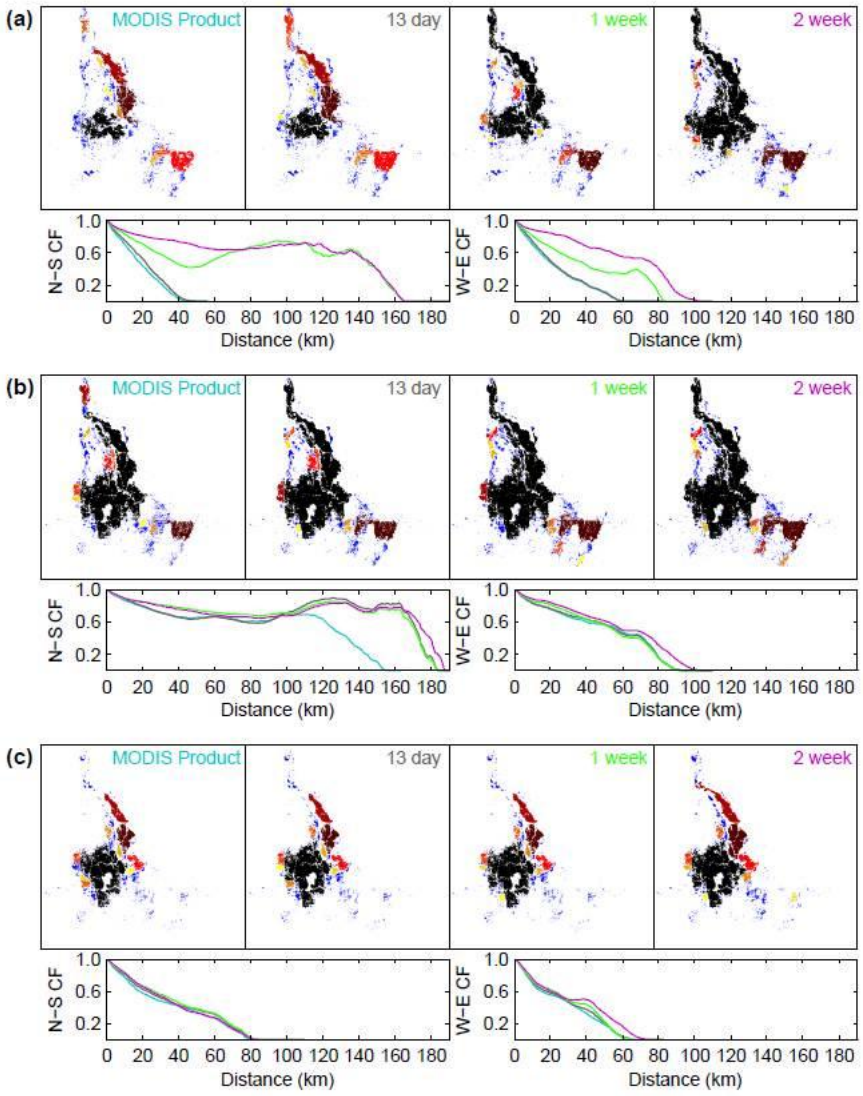

Figure 5 – Connected object plots (top 4 boxes) and associated North-South and West-East connectivity function plots for the MODIS Product, 13 day gap fill, 1 week aggregate and 2 week aggregate datasets. (a) Rising limb on 12 October 2011, day 285, week42; (b) Flood peak on 3 November 2011, day 307, week45; (c) Recession limb on 13 December 2011, day 347, week51. Connected object plots show the top ten largest connected objects coloured individually, with the largest object as black through red and then to yellow for the tenth largest object. All other objects, most of which are very small, are all coloured blue. Connectivity function plot colours match the associated label colours. Connected object plots are orientated with North in the up direction.

Daily plots of connectivity function (Figure 6) indicate that there are important thresholds in the surface water connectivity that are not obvious from static views of the flood extents. These thresholds are evident from clustering of the connectivity function curves for a period of time during the event. Particularly noticeable is the clustering of curves on the recession limb of the event, where the connectivity function reaches zero at around 80 km (N-S) - 85 km (W-E) on the x-axis. This clustering during recession occurs for around 60 days (10 November 2011-10 January 2012) and examination of the corresponding flood extents shows this clustering relates to the large low-lying depression in the centre of the Bangkok basin, which is slowly draining during this time, reducing flood levels but remaining at the same extent.

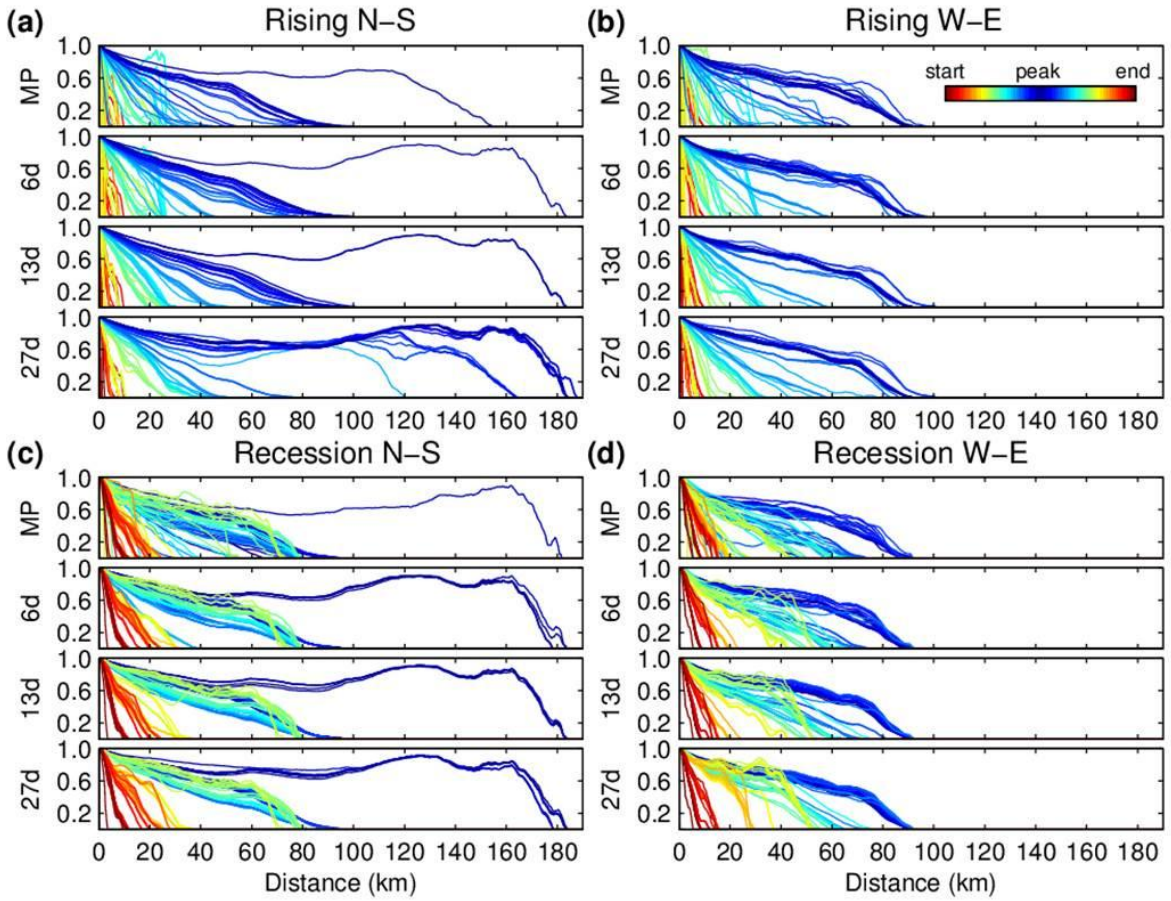

Figure 6 – Daily connectivity function plots for original MODIS product (MP) and 6, 13 and 27 day gap fill length datasets. Connectivity function curves are grouped into four by timing and direction; (a) Rising limb for North-South direction [64 days], (b) Rising limb for West-East direction, (c) Recession limb for North-South direction [100 days], and (d) Recession limb for West-East direction. The start curve is 31 August 2011, peak 3 November 2011, and end curve 11 February 2012.

Comparing results from the different datasets highlights the effect that the different processing, aggregating or gap filling has on the basic connectivity of the inundation data. All the data filling methods result in an increase in connectivity for the three event times, as they all add information to the basic low cloud image data. The 2 week aggregate produces the most connectivity to the point where its rising-limb connectivity function is greater than that of the low cloud peak dataset. Plots of the ten largest disconnected flood areas in each flood extent (Figure 5) show the extra connectivity produced by the filling methods link up areas which in the original data were not connected. This added connectivity is primarily along the main line of flooding N-S in the centre of the image. It is most notable during the more dynamic rising limb, where the flood wave is still moving south, so aggregating over this time has a bigger effect. In contrast, the recession plots show very little change in connectivity, as the flood is consolidating in the low lying and slow draining areas in the centre of the study area, either side of the river. Daily plots of connectivity (Figure 6) show large changes in connectivity function as the event progresses, with connectivity function increasing and decreasing

with no obvious mechanism other than a correlation with the cloudiness. This scatter is most noticeable on the rising limb connectivity functions and reduces as more of the gaps are filled. The 6 day gap fill shows a small reduction in the scatter, but it is not until the 13 day gap fill results that a steady progression in connectivity is observed. The 27 day gap fill dataset also shows a smooth progression in connectivity function, but also includes large increases in for some low cloud days, potentially showing over connectivity for the longer gap fill duration.

Comparing connectivity metadata for the different processed datasets show strong similarities in the overall dynamics indicating these are not likely to be a result of the processing method (Figure 7). Maximum component size (largest wet area) increases proportionately with total flood area. There is a point around week 51-52 where the number of disconnected components drops and coincides with a noticeable mean component size increase. Close inspection of the daily data shows this can be related to the drying or draining of outlying small flood areas that are disconnected from the main flood bodies, leaving the larger ponded flood volumes in lower lying basin areas that remain to be drained.

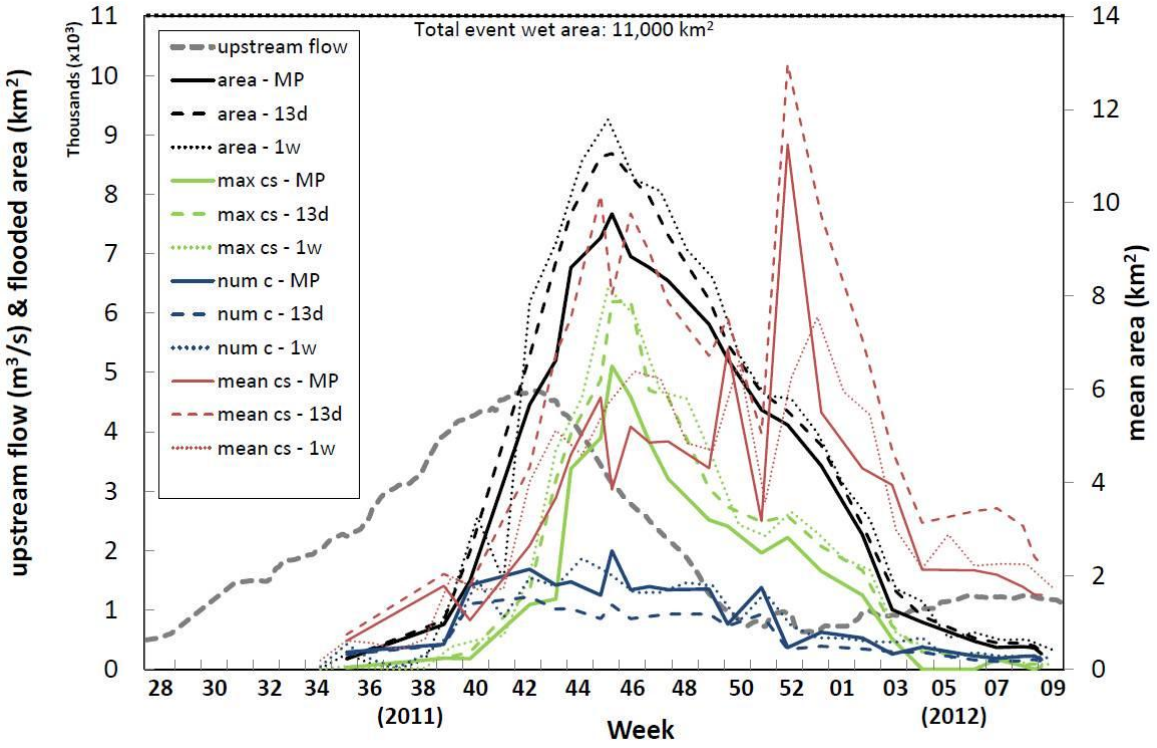

Figure 7 – Connectivity function metadata for three of the analysis datasets. Solid lines for low cloud MODIS product (MP), dashed for 13 day gap fill (13d) and dotted for one week aggregate (1w). Grey dotted is the flow hydrograph, the black lines represent the flooded area, green the maximum component size (max cs), blue is the total number of components (num c), and red is the mean component size (mean cs).

3.3 Gap structure analysis

A Matlab tool was developed that allows the full time series of flood extents to be visualised in three dimensions, with the vertical dimension representing time (Figure 8). In addition to stepping through the two dimensional extents and animation of extents, the tool allows vertical cross-sections through the data to be extracted representing the NS or WE axes along the x axis and time along the y axis (Figure 8 c and d). Gaps are flagged by their length to allow colouring of the gaps by size along with the observed flooded areas. Using this tool, close inspection of the flooded areas shows some missing areas of data from one day to the next that do not appear to be cloud related when

inspected in conjunction with the original MODIS image. These gaps appear, disappear and reappear inconsistently in a manner unlikely to be linked to the dynamics of such a smoothly increasing and decreasing flood event over such a long timescale.

Observed flooding, represented as a blue colour, shows a significant quantity of consistent flood data available from the MODIS product for this event (Figure 8). The days where most or all of the flood extent are missing, are shown as horizontal striping in the cross-sections represented by the corresponding gap colour. The other observation of the gap locations is that there are many data gaps around the periphery of the flooded areas. Finally, plotting cumulative gap count against gap size shows most of the gaps identified in the dataset are of a small size, with ~57% of the total gap count being 6 days or less in length (Figure 8c). Approximately ~78% of the gap count is <= 13 days and 92% of the gap count <= 27 days in length.

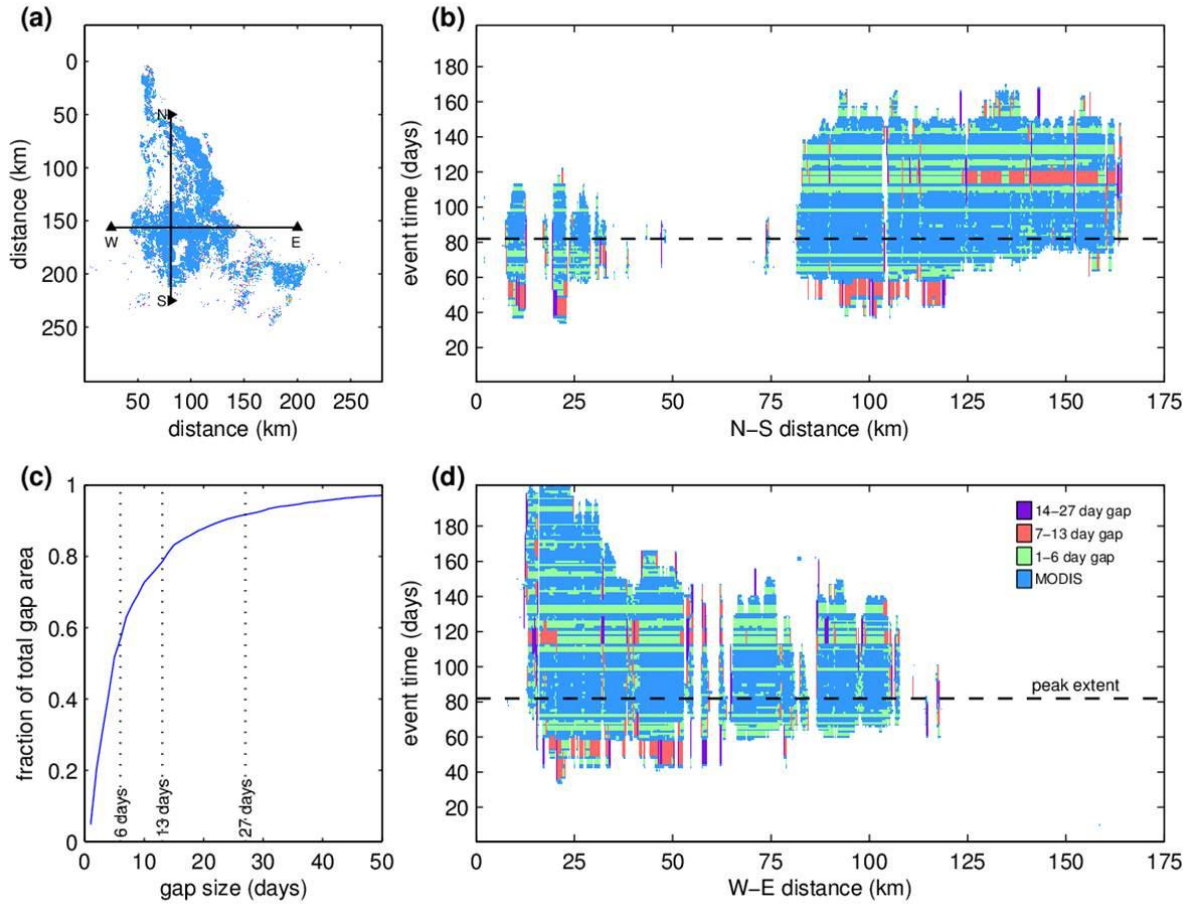

Figure 8 – MODIS product data gap structure. (a) peak extent (day 307, 3 November 2011) showing time-slice locations, (b&d) N-S and W-E time-slice cross-section through event data stack, (c) cumulative fraction of total gap area. Gap lengths used in the processed datasets are illustrated by colour in the time-slices and dotted lines in the gap area plot.

3.4 Spatial scale of observed data

In order to assess the effect of the spatial scale of the observed data on the connectivity function analysis, we compared results from different observation instruments. This comparison used wet-dry binary maps derived from an EO-1 image and MODIS product data for the same day and location (Figure 9 a&b). Flooded area for the overlapping analysis location (5,500 km^2) for the MODIS product and EO-1 were 2,003 km^2 and 1,927 km^2 respectively, a difference of 4%. While the flooded area

from the two datasets is very similar, there are fundamental differences in the connectivity (figure 9). Connected objects plots show underlying differences in what is resolved as connected in the images (figure 9a&b). Whilst the EO-1 image clearly shows the river channels, these are mostly missing from the MODIS data as the channels are ~160-180 m in width and the banks are lined with houses and levees, which other than at breach locations are dry. However, the higher resolution in the EO-1 image also breaks up the surface water connectivity by resolving the strips of housing along the roads (which were flooded internally). While the connectivity method allows for none direct connections (eg around the buildings), if these regions of unobserved connections completely divide a flooded area into smaller areas, this will result in a reduction of the connectivity function. In this case, this results in the lowest resolution image having the highest connectivity. Majority resampling the EO-1 30 m data to 150 m shows a small decrease in N-S connectivity function and an increase in W-E connectivity function (Figure 9e). Resampling the EO-1 30 m data to 250 m shows an increase in N-S connectivity function and in W-E connectivity function (Figure 9f) almost to the same level as that observed in the MODIS product.

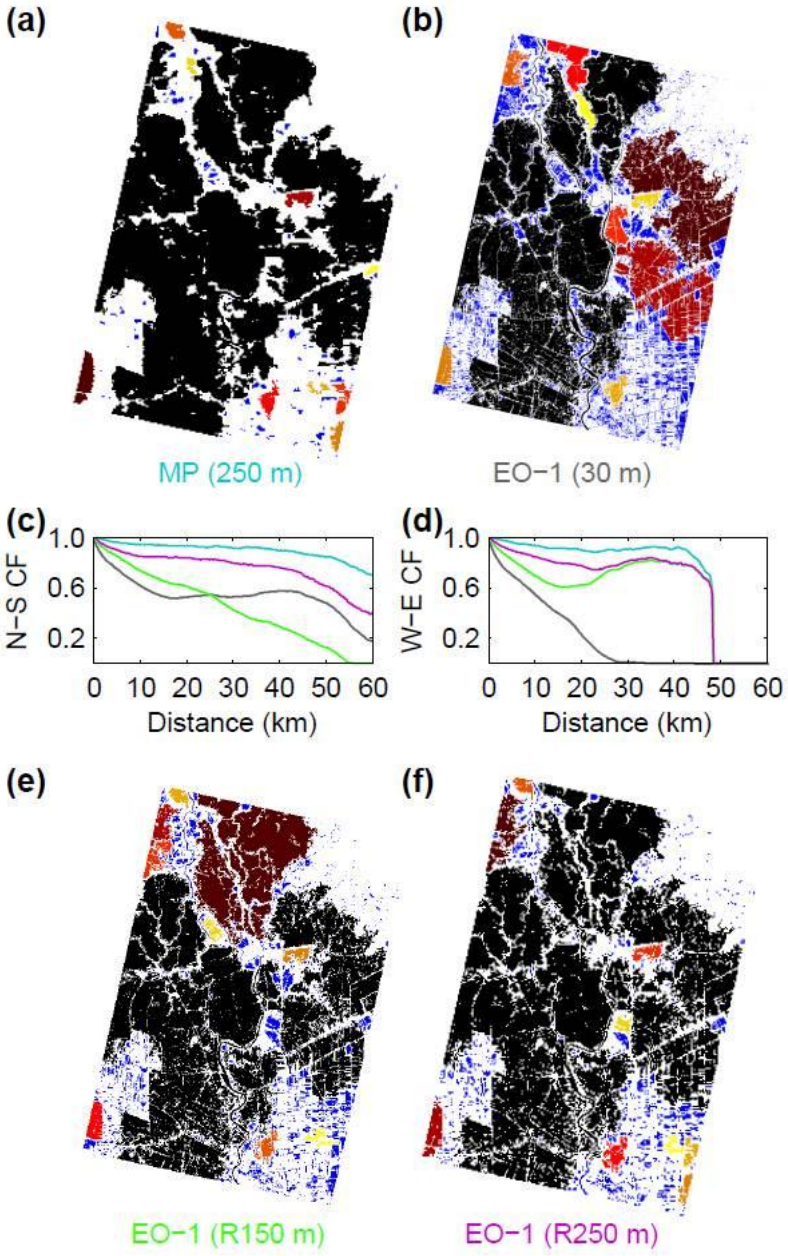

Figure 9 – MODIS product comparison with EO-1 for 26 November 2011. (a, b, e & f) Connected object extent plots for MODIS Product (MP), EO-1 original 30 m resolution, EO-1 resampled to 150m and 250m respectively. (c & d) N-S and W-E connectivity function plots. Connected object plots show the top ten largest connected objects coloured individually, with the largest object as black through red and then to yellow for the tenth largest object. All other objects, most of which are very small, are all coloured blue. Connectivity function plot colours match the associated label colours. The image footprint is 47 km x 117 km.

4 Discussion

4.1 Surface water connectivity

The connectivity analysis of the 2011 flood event in Bangkok demonstrates a clear structure to the dynamics of the event through time and space. The combined river and floodplain surface water connectivity in the North–South direction increased during the rising limb of the event as the flood wave passes through the river reach. This was followed by increasing connectivity on the floodplain in the W-E direction around the event peak, as the low lying basin areas fill. During the recession there was a rapid reduction in N-S connectivity in the first week after the passage of the flood wave peak. This rapid reduction in N-S connectivity contrasted with a slow decrease in the W-E connectivity as the flooded depressions gradually drained reducing flood depth while flood spatial extent remained static for long periods. The movement of a flood wave passing down a river system has been observed with remote sensing data before (e.g. Smith and Pavelsky, 2008; Frazier and Page, 2009; Syvitski et al., 2012), but this is the first time that the effect of its passage on surface water connectivity has been objectively quantified.

There are two key characteristics of the connectivity function curve that can be used to identify important changes in a system. These characteristics are; (i) the distance at which the curve reaches zero, indicating the maximum extent that is connected, and (ii) the shape of the curve, with a concave curve indicating poor internal connectivity within the flooded extent and a convex curve indicating good connectivity. If large changes in these characteristics are observed from one day or week to the next in a time series, this indicates there must be a mechanism which has altered connectivity between the two times. This is observed with the Bangkok flooding where the N-S connectivity function curves (Figure 6a) show step changes in the maximum distance of connection from 80 km to 180 km over a week, as well as increasing curve convexity, that can be correlated with a major levee breach on 24 October 2011, allowing water to progress into the North of Bangkok city. Unplanned structural modifications to flood defences were a notable characteristic of this particular flood event, as there were large amounts of levee construction during the event as well as forced removal of levees by residents trying to prevent increasing flood levels outside protected areas (Yuvejwattana and Suwannakij, 2011).

Where the characteristic of the connectivity function curves do not change much over time, this could indicate the system is in steady state, or that there is a threshold in the system preventing a change in connectivity. We observe such a threshold during the recession period with the clustering of the connectivity function curves for around 60 days (Figure 6c), and this correlates with a period where the large flooded low lying areas in the floodplain are no longer connected to the river through overland flow, but slowly drain through the floodplain channel network. This is similar to phase 5 of the flood sequence described by Zwolinski (1992), where there is a cessation of floodwater transport across the floodplain. Thus through these changes and thresholds in the connectivity, we can see a clear structure to the event progression. These observations demonstrate new insights into flood event dynamics and were not anticipated *a priori*. Changes in the connectivity function provide clear indications of thresholds within the system, and crucially provide a time and location to look for a causal mechanism. The importance of these mechanisms, e.g. overtopping of topographical barriers and flow in floodplain channels, on the dynamics of floodplain inundation is crucial to the modelling of those dynamics in rural (Nicholas and Mitchell, 2003; Bates et al., 2006; Alsdorf et al., 2007) and urban areas (Schumann et al., 2011).

Flood inundation extent varies during the event with a similar triangular shape to that of the upstream flow input. Connectivity analysis shows that this flood extent is a relatively simple reflection of the dynamics occurring during the event, with more detail of the dynamics available when the flood extent is assessed as connected areas. This assessment reveals that during mid-

recession, the number of separately wet floodplain objects reduces and the average area of each object increases identifying the point in the recession where the outer floodplain areas are drying up and consolidating into a few large ponded areas, which are slow to drain. Bates et al. (2006) also showed this falling limb disconnect between channel and floodplain and ponding in a smaller number of floodplain areas for a much smaller floodplain in the UK. This might suggest that this process is common across different scales and climatic regimes.

This marked difference in connectivity function between rising and receding limb dynamics, as well as the observed thresholds, emphasise the different mechanisms for filling (eg. levee overtopping and water moving down slope) and draining (eg. pumped drainage of ponded flood storage) of this type of floodplain. This kind of information may be useful for planning of future infrastructure, but also highlights that flood consequences for Bangkok will be exacerbated by delta subsidence and sea level rise, as well as future development in these areas, irrespective of whether future events are bigger due to climate change or not (Syvitski et al., 2009).

Whilst application of the connectivity function metric is demonstrably useful, we also note that it is sensitive to slight differences in observed flood extent, particularly if those differences occur at locations that result in disconnection of one large flooded area from another. This can be seen with the comparison with the EO-1 image and MODIS. The lower resolution MODIS images are probably better as an overall representation of connectivity than the EO-1 image, as we know from field reports that most of the flooded areas are well connected through the extensive channel network. It is important to consider what flood connectivity is being measured, as even at higher resolution there will still be connectivity that is not in the observed image. This may make it unsuitable to compare a connectivity function from a hydrodynamic model, to a connectivity function from an observed flood extent as what is being compared is fundamentally different. The model may have missing processes which alter the resulting connectivity function, but the output has no missing data. In contrast, the observed flood extent has complete real-world connectivity, but may be missing data or have unobservable detail due to limitations in the observation method, which also resulting in an altered connectivity function.

Geostatistical connectivity proved to be an easily applied tool and an objective way of assessing the large datasets assembled for this study. The sensitivity of the method does make it useful in comparing different processing techniques, where comparisons are relative to the baseline dataset. For example, this means that the method may also be useful for comparing the effect of different Digital Elevation Models (DEMs) resampling techniques on connectivity. It may also be a useful way of assessing the importance of the implementation of the 4 or 8 way connectivity used in different hydrodynamic models. Direction of analysis is also important for the application of the connectivity function and here the N-S orientation allowed a straightforward assessment. If the orientation is not clearly orthogonal, the diagonal connectivity function results will need to be used or a rotation of the grid applied for even more flexibility. Finally, although we confined our analysis here to the overall study area, the connectivity function of different parts of the floodplain could also be usefully compared, such as left and right bank. Resampling tests with the EO-1 image show some sensitivity of the method in application to different scales, even from the same dataset. This undermines the use of geostatistical connectivity as a scale independent tool, however, this sensitivity may be more related to the gridded data structure and resampling methods than the connectivity function itself and will require further investigation.

4.2 Data quality

A pre-processed, global, regular and low latency dataset like the MODIS flood product has real potential to help monitor and understand complex large scale flood dynamics. Much has been said on this in other papers (e.g.Brakenridge and Anderson, 2006; Brakenridge et al., 2012) and the focus

here is on attempting to understand the issues related to using the data to study the detailed spatio-temporal connectivity of a globally important (in terms of damage and loss of life) flood. A key finding in terms of the quality of the product is that missing data is a significant issue when assessing detailed dynamics through an event. This issue with MODIS data is not a new one and is well documented on the NASA download website. However, our biggest criticism of the original vectorised product is that there was no indication of where data were missing, so it was not clear whether a location was dry or just missing data. This has been recognised and explicitly addressed by the provision of a new raster dataset product, available since March 2012, which flags missing data (MODIS Water Product, MWP). Also for users more interested in the overall extent rather than detailed dynamics, composited data over a longer period avoids some of these data gap problems.

Even with the data gap issues we encountered, at the scale of the event being studied, the MODIS product data captures the changing flood extent dynamics. Given the high cloud cover, particularly during the early part of the event, it was impressive that MODIS managed to resolve any flood information at these points. However, these clouds still resulted in long gaps in the data when trying to assess the development of the connectivity on a daily basis. Even low cloud days showed inconsistent discontinuities in connectivity that could be related to the edges of the flooded areas upon examination of the gap structure. This was identified as likely to be related to a pixel changing from wet to dry and back again as it alternates either side of a MODIS processing threshold. Other than a detailed study of the method of generating the wet/dry mask, we will still need to allow for this characteristic.

We have shown that aggregating data to allow for gaps can be useful but can lead to overestimation of the flood extent and an averaging of the daily dynamics that are of interest here, particularly when the aggregation period becomes overly large for the scale of event (i.e. two weeks for Bangkok). We implemented a more subtle method of filling the gaps in the data based on a basic assumption related to flood processes, namely that an area will not usually oscillate between wet and dry repeatedly. The gap fill method is constrained by the information content of the original dataset spatially and so does not artificially combine different spatial areas that are not flooding at the same time, like the aggregation method, i.e. the gap fill method is more true to the observed dynamics. The size of gap, measured in days, which can be reliably filled with this method will be dependent upon the type and duration of the event and how much original data there are. In this event, the allowable gap size could tend towards the higher end due to the extensive flooding, and the long and slow dynamics. An objective method of choosing an appropriate gap length for the fill method and assessing the improvement in quality of the resulting time series would require access to an independent dataset that provides high quality data for cloudy days, such as high resolution SAR or ground based survey.

5 Conclusions

The connectivity for a large scale flood event has been quantified using a geostatistical method applied to a daily remote sensing MODIS product. The connectivity function has been shown to be a reliable and objective method of assessing surface water flood connectivity. The method can be sensitive to small areas of missing data, however, within the same dataset and with a sufficiently robust and thorough analysis, this makes geostatistical connectivity a useful tool for relative comparison of different processing methods. Comparing connectivity of extent data for the same time and location, from different instruments with a large disparity in spatial resolution (MODIS & EO-1) shows that differences in how the flooded area is resolved resulting in fundamentally different connectivity functions, despite the two products showing similar flooded area (4% difference). This implies that using geostatistical connectivity for comparison between different data types, for example observed and modelled extent, will require further investigation to fully understand the implications, particularly if there is a difference in spatial resolution.

This study demonstrates that the MODIS surface water product is a valuable dataset for assessing observed flood dynamics for spatially and temporally large scale events. Provided that allowance is made for the missing data due to clouds and other factors, it can provide useful information. Analysis of the structure of the gaps within the MODIS product, rather than just the data can lead a useful understanding of the quality of the data for a given event and can suggest how best to allow for those gaps. The gap filling method implemented here is a better method for filling the MODIS data gaps than a simple aggregation, as it better preserves the dynamic information of the event while resulting in a complete daily dataset for analysis.

The results of the connectivity analysis demonstrate a clear structure to the dynamics of the event through time and space. Connectivity changes continually throughout the event and the use of daily data allows us to study these dynamics in detail, revealing new insights into flood inundation processes, both for this particular event and perhaps more generally. Specifically, the effect of the passage of the flood wave is directly observable in the progression of out-of-bank flooding, increasing and decreasing connectivity dynamically along the river. During rising water, along river connectivity increases first, followed by an increase in connectivity into the floodplain. There are also sudden increases in connectivity correlated with a major levee breach. During recession, there is a rapid reduction in along river connectivity contrasted with a much slower decrease in the floodplain connectivity, as the flooded depressions gradually drained reducing flood depth while flood spatial extent remained static for long periods (60 days). Analysis of this recession threshold in the floodplain inundation indicates that although spatial flood extent changes are small at this time, there is a reorganisation of the internal connectivity within the overall flooded area. Through these quantified changes and thresholds in the connectivity, we can observe a clear structure to the flood event progression. These observations demonstrate new insights into flood event dynamics that were not anticipated *a priori* and also present the prospect that geostatistical connectivity may provide a new method for quantifying and studying flood inundation.

Acknowledgements

The lead author is a Willis Research Fellow and the research for this paper was completed under funding provided by the Willis Research Network. We are grateful for constructive comments from our anonymous reviewers.

References

Alsdorf, D., Bates, P., Melack, J., Wilson, M., Dunne, T., 2007. Spatial and temporal complexity of the Amazon flood measured from space. Geophysical Research Letters, 34(8): 5.

Auynirundronkool, K. et al., 2012. Flood detection and mapping of the Thailand Central plain using RADARSAT and MODIS under a sensor web environment. Int. J. Appl. Earth Obs. Geoinf., 14(1): 245-255.

Bates, P.D., 2012. Integrating remote sensing data with flood inundation models: how far have we got? Hydrol. Process., 26(16): 2515-2521.

Bates, P.D., Marks, K.J., Horritt, M.S., 2003. Optimal use of high-resolution topographic data in flood inundation models. Hydrol. Process., 17(3): 537-557.

Bates, P.D. et al., 2006. Reach scale floodplain inundation dynamics observed using airborne synthetic aperture radar imagery: Data analysis and modelling. J. Hydrol., 328(1-2): 306-318.

Bracken, L.J., Croke, J., 2007. The concept of hydrological connectivity and its contribution to understanding runoff-dominated geomorphic systems. Hydrol. Process., 21(13): 1749-1763.

Brakenridge, G.R., Kettner, A.J., Slayback, D., Policelli, F., 2012. maps 100E020N and 090E020N, The Surface Water Record. In: Dartmouth Flood Observatory, U.o.C., Boulder, CO, USA (Ed.), http://floodobservatory.colorado.edu/index.html.

Brakenridge, R., Anderson, E., 2006. Modis-based flood detection, mapping and measurement: The potential for operational hydrological applications. In: Marsalek, J., Stancalie, G., Balint, G. (Eds.), Transboundary Floods: Reducing Risks Through Flood Management. NATO Science Series IV Earth and Environmental Sciences. Springer, Dordrecht, pp. 1-12.

Chien, S. et al., 2011. COMBINING SPACE-BASED AND IN-SITU MEASUREMENTS TO TRACK FLOODING IN THAILAND. 2011 Ieee International Geoscience and Remote Sensing Symposium. Ieee, New York, 3935-3938 pp.

Day, G., Dietrich, W.E., Rowland, J.C., Marshall, A., 2008. The depositional web on the floodplain of the Fly River, Papua New Guinea. J. Geophys. Res.-Earth Surf., 113(F1).

Frazier, P., Page, K., 2009. A REACH-SCALE REMOTE SENSING TECHNIQUE TO RELATE WETLAND INUNDATION TO RIVER FLOW. River Res. Appl., 25(7): 836-849.

Gallardo, B., Gascon, S., Gonzalez-Sanchis, M., Cabezas, A., Comin, F.A., 2009. Modelling the response of floodplain aquatic assemblages across the lateral hydrological connectivity gradient. Mar. Freshw. Res., 60(9): 924-935.

Gilvear, D.J., 1999. Fluvial geomorphology and river engineering: future roles utilizing a fluvial hydrosystems framework. Geomorphology, 31(1-4): 229-245.

Jeffiries, R., Darby, S.E., Sear, D.A., 2003. The influence of vegetation and organic debris on flood-plain sediment dynamics: case study of a low-order stream in the New Forest, England. Geomorphology, 51(1-3): 61-80.

Journel, A.G., Kyriakidis, P.C., Mao, S., 2000. Correcting the smoothing effect of estimators: A spectral postprocessor. Math. Geol., 32(7): 787-813.

Junk, W.J., Bayley, P.B., Sparks, R.E., 1989. The flood pulse concept in river floodplain systems. Can. Spec. Publ. Fish. Aquat. Sci., 106: 110-127.

Karim, F., Kinsey-Henderson, A., Wallace, J., Arthington, A.H., Pearson, R.G., 2012. Modelling wetland connectivity during overbank flooding in a tropical floodplain in north Queensland, Australia. Hydrol. Process., 26(18): 2710-2723.

Komori, D. et al., 2012. Characteristics of the 2011 Chao Phraya River flood in Central Thailand. Hydrological Research Letters, 6: 41-46.

Marcus, W.A., Fonstad, M.A., 2010. Remote sensing of rivers: the emergence of a subdiscipline in the river sciences. Earth Surf. Process. Landf., 35(15): 1867-1872.

McFeeters, S.K., 1996. The use of the normalized difference water index (NDWI) in the delineation of open water features. International Journal of Remote Sensing, 17(7): 1425-1432.

McLaren, D., Doubleday, J., Chien, S.V., 2012. Using WorldView-2 imagery to track flooding in Thailand in a multi-asset sensorweb. In: Shen, S.S., Lewis, P.E. (Eds.), Algorithms and

Technologies for Multispectral, Hyperspectral, and Ultraspectral Imagery Xviii. Proceedings of SPIE. Spie-Int Soc Optical Engineering, Bellingham.
Mertes, L.A.K., Dunne, T., Martinelli, L.A., 1996. Channel-floodplain geomorphology along the Solimoes-Amazon River, Brazil. Geological Society of America Bulletin, 108(9): 1089-1107.
Michaelides, K., Chappell, A., 2009. Connectivity as a concept for characterising hydrological behaviour. Hydrol. Process., 23(3): 517-522.
Neal, J. et al., 2011. Evaluating a new LISFLOOD-FP formulation with data from the summer 2007 floods in Tewkesbury, UK. J. Flood Risk Manag., 4(2): 88-95.
Neal, J.C., Schumann, G.J.-P., Bates, P.D., 2012. A sub-grid channel model for simulating river hydraulics and floodplain inundation over large and data sparse areas. Water Resour. Res.
Nicholas, A.P., Mitchell, C.A., 2003. Numerical simulation of overbank processes in topographically complex floodplain environments. Hydrol. Process., 17(4): 727-746.
Pardo-Iguzquiza, E., Dowd, P.A., 2003. CONNEC3D: a computer program for connectivity analysis of 3D random set models. Comput. Geosci., 29(6): 775-785.
Pavelsky, T.M., Smith, L.C., 2008. Remote sensing of hydrologic recharge in the Peace-Athabasca Delta, Canada. Geophysical Research Letters, 35(8).
Pringle, C.M., 2001. Hydrologic connectivity and the management of biological reserves: A global perspective. Ecol. Appl., 11(4): 981-998.
Schumann, G.J.P., Neal, J.C., Mason, D.C., Bates, P.D., 2011. The accuracy of sequential aerial photography and SAR data for observing urban flood dynamics, a case study of the UK summer 2007 floods. Remote Sens. Environ., 115(10): 2536-2546.
Smith, L.C., 1997. Satellite remote sensing of river inundation area, stage, and discharge: A review. Hydrol. Process., 11(10): 1427-1439.
Smith, L.C., Pavelsky, T.M., 2008. Estimation of river discharge, propagation speed, and hydraulic geometry from space: Lena River, Siberia. Water Resour. Res., 44(3).
Smith, M.W., Bracken, L.J., Cox, N.J., 2010. Toward a dynamic representation of hydrological connectivity at the hillslope scale in semiarid areas. Water Resour. Res., 46.
Syvitski, J.P.M. et al., 2009. Sinking deltas due to human activities. Nat. Geosci., 2(10): 681-686.
Syvitski, J.P.M., Overeem, I., Brakenridge, G.R., Hannon, M., 2012. Floods, floodplains, delta plains - A satellite imaging approach. Sediment. Geol., 267: 1-14.
Tockner, K., Malard, F., Ward, J.V., 2000. An extension of the flood pulse concept. Hydrol. Process., 14(16-17): 2861-2883.
Trigg, M.A., Bates, P.D., Wilson, M.D., Schumann, G.J.P., Baugh, C., 2012. Floodplain channel morphology and networks of the middle Amazon River. Water Resour. Res., 48(10).
Ward, J.V., Stanford, J.A., 1995. ECOLOGICAL CONNECTIVITY IN ALLUVIAL RIVER ECOSYSTEMS AND ITS DISRUPTION BY FLOW REGULATION. Regul. Rivers-Res. Manage., 11(1): 105-119.
Ward, J.V., Tockner, K., Schiemer, F., 1999. Biodiversity of floodplain river ecosystems: Ecotones and connectivity. Regul. Rivers-Res. Manage., 15(1-3): 125-139.
Wilson, M. et al., 2007. Modeling large-scale inundation of Amazonian seasonally flooded wetlands. Geophysical Research Letters, 34(15).
Xiao, X.M. et al., 2005. Mapping paddy rice agriculture in southern China using multi-temporal MODIS images. Remote Sens. Environ., 95(4): 480-492.
Xu, H.Q., 2006. Modification of normalised difference water index (NDWI) to enhance open water features in remotely sensed imagery. International Journal of Remote Sensing, 27(14): 3025-3033.
Yuvejwattana, S., Suwannakij, S., 2011. Bangkok Residents Clash as Anger Over Thai Flood Intensifies. Bloomberg News, Bloomberg.com.
Zwolinski, Z., 1992. Sedimentology and geomorphology of overbank flows on meandering river floodplains. Geomorphology, 4(6): 367-379.